Thermal Contraction of Au Nanoparticles

W.-H. Li, S. Y. Wu, C. C. Yang, S. K. Lai, and K. C. Lee
Department of Physics, National Central University, Chung-Li, Taiwan 32054, Republic of China

H. L. Huang and H. D. Yang
Department of Physics, National Sun Yat-Sen University, Kaohsiung, Taiwan 804, Republic of China
(Received 17 April 2002; published 5 September 2002)

A fine Au powder, with a mean particle diameter of 4 nm, has been successfully fabricated. The crystalline structure of the 4 nm Au nanoparticles remains in fcc symmetry. No structural changes were found between 15 and 450 K. A crossover from a positive thermal expansion at low temperatures to a negative thermal expansion at high temperatures was observed in the fcc cell parameter at about 125 K. Anomalies associated with the crossover were also observed in the magnetic response and the heat capacity measurements. The observations can be reasonably well interpreted by accounting for the effects of the valence electron potential on the equilibrium lattice separations, with a weakly temperature dependent level spacing.

DOI: 10.1103/PhysRevLett.89.135504 PACS numbers: 81.07.Wx, 81.16.Be, 85.85.+j

Thermal expansion is normally observed in most materials. This behavior can be understood by accounting for the effects of the anharmonic lattice potential on the equilibrium lattice separations and is usually characterized by the Grüneisen parameter [1] in terms of a linear expansion coefficient, $\alpha \equiv \frac{1}{a}(\frac{\partial a}{\partial T})_P$, where a is the lattice parameter. Negative thermal expansion, which represents lattice contraction upon heating, is not uncommon among anisotropic systems, where contraction along one crystallographic direction is usually accompanied by expansion along the others [2]. For isotropic systems, it is frequently associated with a structural distortion related to anisotropic lattice excitations [3]. In most cases, negative thermal expansion occurs in only a narrow temperature range. In this Letter, we report on the observation of a crossover from a positive thermal expansion at low temperatures to a negative thermal expansion at high temperatures in cubic Au nanoparticles, where no structural changes have occurred.

Au nanoparticle powder was fabricated by employing the gas condensation method. High-purity gold ingots (99.999%) were evaporated in an Ar atmosphere at a pressure of 0.8 torr, using an evaporation rate of 0.1 Å/s. A stainless steel plate, maintained at the liquid nitrogen temperature, was used to collect the evaporated particles. After restoration to room temperature, the powder, which is only loosely attached on the collector, was stripped off. The resultant powder was no longer gold yellow but dark black, indicating that the absorption band of the powder had blueshifted to the invisible region, as most metallic nanoparticles do. The sample was in a powder form, consisting of a collection of individual Au nanoparticles. There is no substrate. The sample was quite stable against exposure to the air, but was sensitive to heat. However, the data shown in this Letter were all obtained on the sample that was kept in isolation from the air at all times.

X-ray diffraction and atomic force microscopy (AFM) were used to characterize the powder. Figure 1(a) shows the x-ray diffraction pattern of the powder (bottom) and of the ingot used for evaporation (top). As expected, the diffraction peaks of the powder are much broader than those of the ingot, reflecting the finite-size effect. A portion of the AFM images and the size distribution, obtained from a 1 μm $\times$ 1 μm image, are shown in

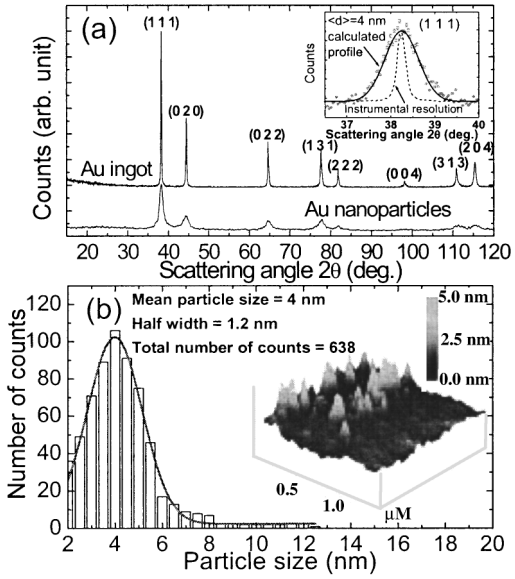

FIG. 1. (a) The x-ray diffraction patterns, taken at room temperature, of the nanoparticles and the ingot. Line broadening, resulting from the finite-size effect, can be clearly seen in the nanoparticle pattern. The inset shows the observed (circles), fitted (solid curve), and instrumental resolution (dashed curve) profiles for the {111} reflection. (b) A portion of an AFM image of the nanoparticle powder. A symmetrical size distribution is obtained which may be described by using a Gaussian distribution function, indicated by the solid curve.

Fig. 1(b). This image was obtained by very loosely spreading the nanoparticles onto a glass slide and was taken using a Digital Instruments Nanoscope III, operated in the tapping mode. A quite symmetrical size distribution was obtained, which could be described using a Gaussian function (shown as the solid curve on the data), with its center at 4 nm and a half-width at 1.2 nm. Using the peak profiles of the ingot as the instrumental resolution [shown as the dashed curve in the inset of Fig. 1(a)] and assuming a Gaussian size distribution of half-width 1.2 nm, we obtained a mean particle diameter of 4.0(4) nm for the powder, by fitting the nanoparticle pattern to the diffraction profiles of finite-size particles. One of the calculated profiles is shown as the solid curve in the inset of Fig. 1(a). Apparently, the mean diameter obtained from the x-ray pattern and from the AFM images agrees well.

Although it is commonly expected that the structure of finite-size particles may differ from those of the bulk system [4,5], the crystalline structure of the 4 nm Au nanoparticles remains in fcc symmetry, as the Au ingot does. The room temperature cell parameter of the nanoparticle ($a = 4.0682$ Å) is ~0.2% smaller than that of the ingot ($a = 4.0761$ Å). A similar contraction of the atomic separation of the nanoparticles, originating from the size effect, has also been observed [6,7] in other nanostructure systems. This behavior has been attributed [6] to an increase in the surface stress in nanoparticles, due to the high value of their surface to volume ratio. Note that there are ~4600 Au atoms in the 2.4 nm fcc nanoparticles, of which ~13% are on the surface. A larger size contraction can be expected in smaller nanoparticles [7]. No diffraction peaks from other than the fcc Au were observed in the nanoparticle powder; in particular, no obvious signals from the oxidation on the surface were found, as was expected. No structural changes were found for nanoparticles between 15 and 450 K. Thermal interparticle fusion becomes significant when the nanoparticles are heated above 400 K. Figure 2 shows the temperature dependence of the nanoparticle cell parameter for temperatures below 390 K. The open and solid symbols indicate the data from two separate experiments. Below 100 K, a positive thermal expansion is seen, with a linear expansion coefficient of $\alpha = +3.2 \times 10^{-5}\ \mathrm{K}^{-1}$, which is a factor of 2.3 times larger than that of the bulk Au ($\alpha = +1.4 \times 10^{-5}\ \mathrm{K}^{-1}$) [8], signifying the existence of effects due to excitations other than from the lattice. A downturn in the temperature dependence of the cell parameter occurs at about 125 K. Above 150 K, the linear expansion coefficient becomes negative ($\alpha = -2.5 \times 10^{-5}\ \mathrm{K}^{-1}$), showing lattice contraction, rather than expansion, upon heating. Note that normal positive thermal expansion was observed [9,10] in nanoscale Au grains deposited on carbon substrate. In these so-called "island film" systems, the interactions between the grains and the substrate can be important, which may result in a weakening of the apparent size effects of the grains themselves.

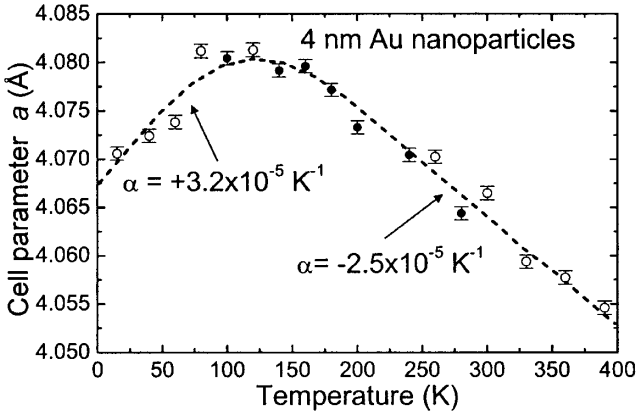

FIG. 2. Temperature dependence of the fcc cell parameter of the Au nanoparticles. A crossover from a positive thermal expansion at low temperatures to a negative thermal expansion at high temperatures is seen at about 125 K. The open and solid symbols indicate the data from two separate experiments.

To delve further into the origin of the above anomaly, the magnetic responses and the heat capacity of the system were also measured. The temperature dependencies of the magnetic responses to a weak ac magnetic field, with an rms strength of 1 Oe and a frequency of 100 Hz, for the nanoparticles (solid symbols) and for the ingot (open symbols), are shown in Fig. 3(a). These data were collected on a Quantum Design physical property measurement system, without the presence of an external magnetic field, but with a 1 Oe probing field. Diamagnetic responses were observed for the ingot at all temperatures, as expected, whereas the nanoparticles showed paramagnetic responses, with a clear peak at around 160 K. The relative heat capacity of the nanoparticles, measured by employing an ac calorimeter using a low frequency chopped laser as the heat source, reveals two small anomalies, which are shown in Fig. 3(b). In the temperature regime studied, huge contributions to the heat capacity from phonons can be expected. The identification of small contributions from other types of excitations as distinct from the phonon contribution is usually difficult. Nevertheless, these are clearly revealed in the dC/dT versus T plot shown in the inset of Fig. 3(b), where definitive changes in dC/dT can be seen at 125 and 155 K. Note that these are the temperatures where cell parameters and magnetic responses show anomalies.

The above observations can be described reasonably well by accounting for the effects of electronic excitations on the equilibrium lattice separation. For bulk systems, where the band separations near the Fermi surface are considerably larger than the thermal energy (a few meV), the electronic effects become noticeable only at relatively high temperatures. In nanoparticles, where discrete levels are separated by only a few meV [11–13], the effects can be significant even at ordinary temperatures. Here, we consider the effects of the valence electron potential on the equilibrium lattice separation in systems (specifically for nanoparticles) having discrete electronic energy

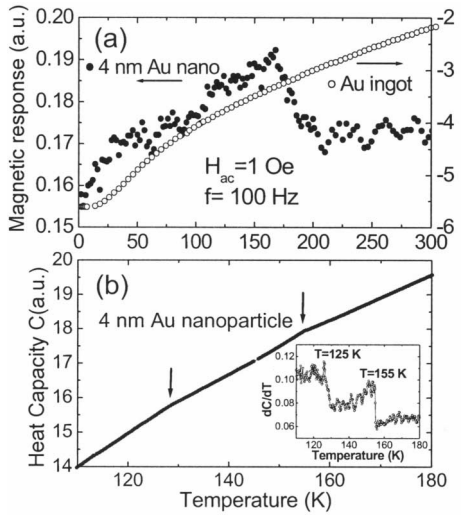

FIG. 3. (a) Temperature dependence of the magnetic response of the Au nanoparticles and the ingot to a weak ac probing magnetic field. Diamagnetic responses for the ingot can be noted, while paramagnetic responses, with a clear peak at about 160 K, are revealed for the nanoparticles. (b) Variation of the heat capacity of Au nanoparticles with temperature. Two anomalies are clearly revealed in the dC/dT versus T plot shown in the inset.

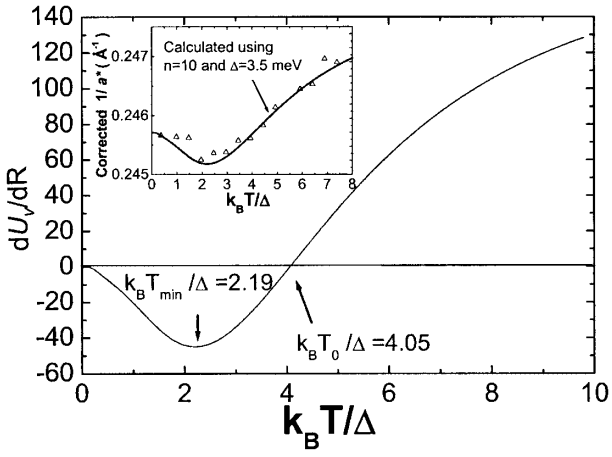

FIG. 4. Plot of the variation of dU_ν/dR with temperature. A minimum occurs at $T_{\min} = 2.19\Delta/k_B$, indicating that the effects on the equilibrium lattice position are different for temperatures below and above $T_{\min}$. The inset shows the temperature dependence of the lattice-contribution-corrected cell parameter. The solid line indicates a theoretical curve based on the expression discussed in the text with $\Delta = 3.5$ meV.

levels. It is known that the allowed energies for valence electrons in nanoparticles can be taken as being inversely proportional to the cube of the particle diameter, which may vary with temperature. A temperature dependent level spacing is then to be anticipated for these spatially confined valence electrons. In terms of the unit cell parameter $R(T)$, the energy of the nth level above the Fermi energy, for a cubic crystalline structure, may then be taken to be $\Delta_n(T) = \alpha_n/R^3$, where α_n depends on the distribution of the levels [11]. Accordingly, the attractive binding energy of thermally excited valence electrons embedded in a cubic lattice of ions, at a finite temperature, is taken to be approximately $U_\nu = -N_e \sum_n \Delta_n(R) f(\Delta_n)$, where N_e is the number of valence electrons and $f(\Delta_n) = \frac{\exp(-\Delta_n/k_BT)}{\sum_m \exp(-\Delta_m/k_BT)}$ is the Fermi-Dirac population function of the nth level. The requirement of an energy minimum for equilibrium atomic separations reads $[\frac{d(U_0+U_\nu)}{dR}]_{R=a} = 0$, where U_0 is the electrostatic energy of the metallic nanoparticles at $T = 0$ and a is the equilibrium lattice constant. Apparently, the second term accounts for the correction of the valence electron energy on the equilibrium lattice positions. It originates from the binding potential of the excited valence electrons in the electrostatic field of the ion cores. Figure 4 shows the variation of the second term with temperature, for an equal spacing ($\Delta_n = n\Delta$) ten-level system [14]. A minimum occurs at $T_{\min} = 2.19\Delta/k_B$, indicating that the effects on the lattice parameters are different for temperatures below and above $T_{\min}$. A crossover from a positive thermal expansion to a negative thermal expansion can then be anticipated at $T = 2.19\Delta/k_B$. Another characteristic temperature of interest is $T_0 = 4.05\Delta/k_B$, at which $dU_\nu/dR = 0$. This is the temperature at which U_ν reaches its maximum, but no correction to the equilibrium lattice positions from the excited valence electrons is made.

For the data shown in Fig. 2, we believe, however, that both the lattice and the valence electrons will contribute to the thermal behavior of the cell parameter. Unfortunately, no data on the lattice expansion coefficient of Au nanoparticles is available. As a reasonable estimate, we adopt the expansion coefficient of the ingot [8] for that of the nanoparticle. The inset of Fig. 4 shows the temperature dependence of $1/a^*$, where a^* is the cell parameter corrected for the lattice contribution by using a linear expansion coefficient of $+1.4 \times 10^{-5}$ K^{-1}. The solid line indicates the theoretical curve for $\Delta = 3.5$ meV, taking the data obtained at the lowest temperature as the reference point for dU_0/dR. This value of $\Delta = 3.5$ meV obtained for 4 nm Au particles agrees well with the 3.24 meV predicted by using Kubo theory [10,15]. We remark that using a temperature dependent Δ in the fit produces essentially no difference in the results, since the variation of Δ with temperature is $\sim$1%, according to the data shown in Fig. 2.

Knowing that the paramagnetic response is proportional to the difference between the spin-up and the spin-down populations, it is reasonable to expect that the maximum paramagnetic response will appear at the temperature at which the thermally excited population reaches its maximum. This temperature can be taken to be at $T = T_0 = 4.05\Delta/k_B$, because the variation of Δ with temperature is only $\sim$1% and the maximum population and the maximum U_ν should occur at essentially the same temperature. Using the same $\Delta = 3.5$ meV $\approx$ 40.6 K as that obtained from the cell parameter data, the maximum paramagnetic response will then be expected

to be at $40.6 \times 4.05 = 164$ K, which agrees very well with the data shown in Fig. 3(a).

Thermal lattice contractions originating from structural changes have been observed in many systems [16,17]. This is, however, not what occurs in the present 4 nm fcc Au nanoparticles, since no structural changes were observed in the temperature regime studied. Lattice shrinking results in an increase in the level separation when the temperature is increased, which, on the one hand, reduces the number of electrons occupying the excited states as dictated by the Fermi-Dirac factor and, on the other hand, raises the thermal energy of individual electrons in the excited states. These two factors compete delicately to achieve a lower electronic potential energy that results in the crossover from thermal expansion to thermal contraction. There may possibly be other effects that might be just as significant. Effects resulting from surface stress, from surface phonons, from finite-size modified lattice potential can all be significant in nanoparticles. Further theoretical investigations along these lines are needed to clarify their effects on the equilibrium lattice separations.

This work was supported by the National Science Council of the Republic of China under Grants No. NSC 90-2112-M-008-043 and No. NSC 90-2112-M-008-045.

[1] N.W. Ashcroft and N. D. Mermin, *Solid State Physics* (Saunders, Philadelphia, 1976), Chap. 25.
[2] A. C. Baily and B. Yates, J. Appl. Phys. **41**, 5088 (1970).
[3] G. K. White, Contemp. Phys. **34**, 193 (1993).
[4] L. D. Marks, Rep. Prog. Phys. **57**, 603 (1994).
[5] C. L. Cleveland, U. Landman, T. G. Schaaff, M. N. Shafigullin, P.W. Stephens, and R. Whetten, Phys. Rev. Lett. **79**, 1873 (1997).
[6] H. Purdum, P. A. Montano, G. K. Shenoy, and T. Morrison, Phys. Rev. B **25**, 4412 (1982).
[7] A. Balerna, E. Bernieri, P. Picozzi, A. Reale, S. Santucci, E. Burattini, and S. Mobilio, Phys. Rev. B **31**, 5058 (1985).
[8] *A Physicist's Desk Reference*, edited by H. L. Anderson (AIP, New York, 1989), 2nd ed., p. 345.
[9] J. S. Vermaak and D. Kuhlmann-Wilsdorf, J. Phys. Chem. **72**, 4150 (1968).
[10] C. Solliard and M. Flueli, Surf. Sci. **156**, 487 (1985).
[11] See, for example, W. P. Halperin, Rev. Mod. Phys. **58**, 533 (1986).
[12] S. Gueron, M. M. Deshmukh, E. B. Myers, and D. C. Ralph, Phys. Rev. Lett. **83**, 4148 (1999).
[13] D. Davidovic and M. Tinkham, Phys. Rev. Lett. **83**, 1644 (1999).
[14] Ten levels above the Fermi level are included in the calculation, so that the population at higher levels is less than 3% even at the temperature with $k_B T = 3\Delta$.
[15] R. Kubo, J. Phys. Soc. Jpn. **17**, 975 (1962).
[16] A. P. Ramirez and G. R. Kowach, Phys. Rev. Lett. **80**, 4903 (1998).
[17] N. Marzari, D. Vanderbilt, A. De Vita, and M. C. Payne, Phys. Rev. Lett. **82**, 3296 (1999).